

ADVANCES IN MULTI-DIMENSIONAL SIMULATION OF CORE-COLLAPSE SUPERNOVAE *

F. DOUGLAS SWESTY AND ERIC S. MYRA †

*Dept. of Physics & Astronomy,
State University of New York at Stony Brook
Stony Brook, NY 11794–3800, USA
E-mail: dswesty@mail.astro.sunysb.edu
emyra@mail.astro.sunysb.edu*

We discuss recent advances in the radiative-hydrodynamic modeling of core collapse supernovae in multi-dimensions. A number of earlier attempts at fully radiation-hydrodynamic models utilized either the grey approximation to describe the neutrino distribution or utilized more sophisticated multigroup transport methods restricted to radial rays. In both cases these models have also neglected the $O(v/c)$ terms that couple the radiation and matter strongly in the optically thick regions of the collapsed core. In this paper we present some recent advances that resolve some shortcomings of earlier models.

1. Introduction: The Supernova “Problem”

For over a decade researchers have struggled to model the convective post-bounce epoch of core collapse supernovae. The radiative-hydrodynamic flows that occur in the region below the stalled prompt shock have held both promise and pitfall for the supernova modeler. The promise of this phenomenon is that it might explain the long sought-after mechanism that converts the core bounce into the observed explosion. The pitfalls are legion, mostly involving a complex convective flow structure that is three-dimensional in nature and couples neutrinos to matter strongly. For this reason there remain many open issues in modeling the convective epoch of core collapse supernovae.

The supernova “problem” persists, despite more than four decades of concentrated research. The problem is this: We have no convincing explanation as to how the core collapse, which ends the evolution of a massive star, rebounds in such a way as to generate the explosion we observe in nature. The most realistic supernova models collapse and rebound, but create a shock wave that doesn’t eject matter, either on the hydrodynamic timescale (~ 10 ms), or the diffusive timescale of the escaping neutrino radiation (~ 1 – 10 s), or on any other timescale we can model.

This is not a problem of overall energetics. The gravitational energy released during core collapse and the subsequent neutron-star cooling phase is several factors of 10^{53} erg. In contrast, the kinetic energy of the explosion required for consistency with observation is only 10^{51} erg. Instead of insufficient energy, the problem is one of energy conversion and transport—how a sufficient portion of the released gravitational energy is imparted to the material *ejectus*, giving it the requisite kinetic energy.

*To appear in published proceedings of *Open Issues in Core-Collapse Supernovae*, which was conducted at The Institute for Nuclear Theory, University of Washington, Seattle, WA, USA, June, 2004.

† Visiting Fellows, The Institute for Nuclear Theory, University of Washington, June, 2004.

It has been understood for many years that neutrinos play a vital role in this process. In fact, essentially the entire remaining 99% of released energy (that which is not converted to kinetic energy of the matter) is radiated away as neutrinos. Thus, an accurate treatment of neutrino processes is a necessary component of any realistic model for a supernova.

In this article, we present what we currently regard as the most important issues in core-collapse supernova modeling. In Sec. 2, we discuss the major components that need to be part of any serious modeling endeavor. In Sec. 3, we present an outline of V2D, our new two-dimensional (2-D) supernova simulation code. Section 4 contains some preliminary results using this code. Our conclusions are in Sec. 5.

2. The Components of a Supernova Simulation

Broadly speaking, there are four main components to current supernova simulation models: (1) hydrodynamics, to track the collapse, rebound, and ejection of stellar material, (2) neutrino transport, to track the production of neutrino radiation and to follow its propagation and emission from the star, (3) nuclear microphysics, to describe the diverse states of matter encountered throughout a simulation, and (4) neutrino microphysics, to describe the reactions and interactions involving neutrinos and matter. It must be stressed that all of these components are tightly coupled to one another. Thus, the most effective models are designed with this coupling built in *ab initio*.

Hydrodynamics. For simplicity of implementation, it has been customary for supernova codes to employ explicit hydrodynamics, with either a Newtonian or a general relativistic formulation. Implicit algorithms have usually been avoided since they require the computationally expensive solution of large systems of non-linear equations.

Regardless of which approach is used, the hydrodynamic portion of the problem requires solution of some form the following equations, expressed here in Newtonian formalism:

$$\frac{\partial \rho}{\partial t} + \nabla \cdot (\rho \mathbf{v}) = 0 \quad (1)$$

$$\frac{\partial (\rho Y_e)}{\partial t} + \nabla \cdot (\rho Y_e \mathbf{v}) = -m_b \sum_f \int d\varepsilon \left(\frac{\mathbb{S}_\varepsilon}{\varepsilon} - \bar{\mathbb{S}}_\varepsilon \right) \quad (2)$$

$$\frac{\partial E}{\partial t} + \nabla \cdot (E \mathbf{v}) + P \nabla \cdot \mathbf{v} = - \sum_f \int d\varepsilon (\mathbb{S}_\varepsilon + \bar{\mathbb{S}}_\varepsilon) \quad (3)$$

$$\frac{\partial (\rho \mathbf{v})}{\partial t} + \nabla \cdot (\rho \mathbf{v} \mathbf{v}) + \nabla P + \rho \nabla \Phi + \nabla \cdot \left\{ \sum_f \int d\varepsilon (P_\varepsilon + \bar{P}_\varepsilon) \right\} = 0. \quad (4)$$

Equation (1) is the continuity equation for mass, where ρ is the mass density and \mathbf{v} is the matter velocity, and where these quantities, and those in the following equations, are understood to be functions of position \mathbf{x} and time t . Equation (2) expresses the evolution of electric charge, where Y_e is the ratio of the net number electrons over positrons to the total number of baryons. In the presence of weak interactions, the right hand side is non-zero to account for reactions where the number of electrons can change. Here, we express the net emissivity of a neutrino flavor (of energy ε) and its antineutrino by \mathbb{S}_ε and $\bar{\mathbb{S}}_\varepsilon$, respectively. This expression is integrated over all neutrino energies and summed over all neutrino flavors f . The mean baryonic mass is given by m_b . Evolution of the

internal energy of the matter is given by the gas-energy equation, Eq. (3), where E is the matter internal energy density and P is the matter pressure. Again, the right hand side of this equation is non-zero whenever energy is transferred between matter and neutrino radiation as a result of weak interactions. We note that it is also possible to substitute for Eq. (3) an expression for the evolution of the *total* matter energy (internal plus kinetic plus potential). Finally, Eq. (4) expresses gas-momentum conservation, where Φ is the gravitational potential, and P_ϵ and \bar{P}_ϵ are radiation-pressure tensors for each energy and flavor of neutrino and its anti-neutrino, respectively.

These equations must be discretized for solution within a computational framework. Traditionally, with one-dimensional models, it has been convenient to use Lagrangean methods, in which a computational mesh strictly co-moves with the mass elements of the fluid. With the advent of multi-dimensional models, however, it is common to use Eulerian hydrodynamics, where the mesh is fixed in an inertial frame of reference. This is because purely Lagrangean methods are difficult to implement in multi-dimensional schemes without the mesh suffering distortion and entanglement in convectively active regions.

For all the benefits of Eulerian meshes, they also present a number of thorny issues. This is especially true for spherical polar meshes, the most natural choice for supernova modeling. The most obvious issue is the coordinate singularity that exists when the polar angle, $\theta \rightarrow 0$. In addition, polar meshes exacerbate the problem of the timestep-restricting Courant-Friedrichs-Levy (CFL) condition at the center of the core. To deal with these issues, there are numerous resolutions and combinations of resolutions under active consideration. These include implicit methods, unstructured meshes, body-fitted meshes, and adaptive mesh refinement (AMR).

As mentioned above, it is also necessary to choose between a total energy and an internal energy formulation. For the supernova problem, an internal energy formulation, as given in Eq. (3), is preferred. This is because much of the energy is internal, as opposed to kinetic. Solving the gas-energy equation helps insure an accurate calculation of the entropy, which is critical in degenerate regimes where a small change in energy can lead to a large change in temperature.

The hydrodynamic algorithm must also have convergence properties that can deal with a realistic equation of state. This is particularly important in the regions of non-convex phase changes, such as the transition between nuclei and continuous nuclear matter.

Neutrino Transport. This component is the most difficult to implement in a supernova model and the most time-consuming computationally. This is because supernova neutrinos cannot, in general, be described by an equilibrium distribution function. A solution requires a complete phase-space description of each neutrino's position and momentum. To obtain such a solution, one must solve the six-dimensional Boltzmann Transport Equation or some reasonable approximation thereof. This extra dimensionality easily leads to the transport calculation completely dominating a simulation in terms of computer memory, execution time, and I/O requirements.

The Boltzmann Transport Equation (BTE) can be expressed in terms of the radiation intensity, $I = I(\epsilon, \mathbf{x}, \mathbf{\Omega}, t)$, where ϵ is the energy of a neutrino, \mathbf{x} its position, and $\mathbf{\Omega}$ the solid angle into which the neutrino radiation is directed. In terms of I , the Newtonian BTE can be expressed as

$$\frac{1}{c} \frac{\partial I}{\partial t} + \mathbf{\Omega} \cdot \nabla I + \sum_i a_i \frac{\partial I}{\partial p_i} = \left(\frac{\partial f}{\partial t} \right)_{\text{coll}}, \quad (5)$$

where a_i is the i^{th} component of the matter acceleration and p_i the i^{th} component of the momentum of the neutrino. The right hand side of Eq. (5) lumps together the contributions from all interactions that a neutrino might experience and is collectively referred to as the collision integral.

A storm of issues faces one who implements a neutrino transport algorithm. Mezzacappa and

Bruenn¹⁸ have the only “full” solution to the BTE implemented in supernova simulations and then only with one-dimensional hydrodynamics. Upon moving to multi-dimensional models, the full solution of the BTE becomes yet more challenging to implement and more time-consuming to compute. However, this is the way that the field must ultimately go. (Livne and colleagues purport¹⁷ to implement a two-dimensional S_n solution of the BTE. However, this solution omits critical matter-radiation coupling terms and no numerical details of the method have been disclosed.)

In the meantime, a number of approximate transport moment methods have emerged. The most successful of these is use of a finite series of angular moments of the BTE. When this approach is taken, a limiting scheme is then required to close the resulting equations. Bruenn² implemented a P_1 scheme, with flux-limiting. Myra *et al.*²¹ closed the zeroth angular moment of the BTE by implementing the Levermore and Pomraning flux limiter¹⁶. Bowers and Wilson¹ also used a flux-limiting scheme of their own device. More recently, Rampp and Janka²² have implemented a variable-Eddington-factor approach to solve the first two angular moments of the BTE. In all the above cases, however, the implementation has been made in only one spatial dimension. (Janka *et al.*¹² are developing a two-dimensional Boltzmann transport code (MuDBaTH), but the numerical details are as yet unpublished.)

Since all the schemes noted so far derive monochromatic transport equations, yielding a separate equation for each neutrino energy, they are referred to as multi-group schemes. Those that combine multi-group and flux-limiting are known as multi-group flux-limited diffusion (MGFLD) schemes.

A much simpler alternative to multi-group schemes is so-call “grey” transport, which is derived by integrating the BTE over both neutrino energy and angle. To perform these integrals, one must assume a spectral shape for the neutrino distribution. Typically, this requires defining an arbitrary neutrino “temperature,” and assuming that neutrinos can be parameterized by some kind of equilibrium Fermi-Dirac distribution. Among relatively recent models, this was first implemented by Cooperstein, van den Horn, and Baron,⁷ and later by Swesty²⁹ and by Herant *et al.*¹⁰ This approximation is still in active use by the latter group.⁹

Grey schemes have numerous shortcomings. First, work with multi-group schemes has shown that in areas where accurate neutrino transport is critical, neutrinos do not assume any kind of distribution that can be parameterized once and for all as required by grey transport. Spectral distributions constantly evolve and, thus, a multi-group description is required to obtain even a qualitatively correct description. More troubling, Swesty²⁹ has shown that by adjusting the grey parameterization within very small bounds, it is possible to “dial” an explosion (or failed explosion) with the appropriate choices of these unknowable and unphysical tuning parameters. Hence, although grey codes have utility for making a sweeping exploration of parameter space, any scientific conclusions that rely on them should be viewed as highly suspicious, and not regarded as in any way definitive.

Regardless of which transport scheme is implemented, another critical issue that must be faced is matter-radiation coupling. Coupling occurs in Eqs. (2)–(4) for lepton number, energy, and momentum evolution. Coupling that occurs on the right-hand side of these equations has a conceptually simple analytic structure. However, momentum transfer is more troublesome in approximate schemes. This is because the radiation momentum equation is often truncated in a way that makes the accuracy of the calculated momentum transfer less certain.

Matter-radiation coupling also enters implicitly in the neutrino transport equation through spectral rearrangement terms and in the dynamic diffusion term. Both these terms are frequently and erroneously neglected in supernova models, even though the dynamic diffusion term is the leading

order contribution in optically-thick regions.

Equation of State. Adequate modeling of stellar-core collapse requires an equation of state (EOS) that handles a density range of roughly 10^5 – 10^{15} g cm⁻³, a temperature range of 0.1–25 MeV, and an electron-fraction range of 0.0–0.5. The EOS must also be able to handle different regimes of equilibrium states. Throughout most of the core, the material is in nuclear statistical equilibrium (NSE) and is usually modeled by one of the NSE equations of state. Although the gross features of nuclear matter are thought to be well-understood, there is still much open ground for investigation. Fertile regimes for such work include the EOS at supernuclear densities. In addition, little is known about the nature of nuclei at subnuclear densities when Y_e is small.

Matter in the silicon shell and beyond does not attain NSE until the bounce-shock wave passes through it. Dealing with the transition between NSE and non-NSE EOS's and with the network of nuclear reactions that joins them is a challenge that is only beginning to be addressed.¹¹

Neutrino Microphysics. Since the energetics of a core-collapse supernova is primarily a neutrino phenomenon, it is necessary to have correct opacities and rates for the various neutrino processes that are important. The collection of reactions that are important, or possibly important, to the supernova problem is rich and has evolved through the years. Arguably the most important development came with the discovery of weak neutral currents, from which it could be inferred that the dominant contribution to neutrino opacity in a collapsing stellar core is from coherent elastic scattering of neutrinos from nuclei.⁸

The list of possible neutrino interactions is nearly endless, but those of demonstrated importance include the coherent scattering just mentioned, as well as conservative scattering from free nucleons. Also of undisputed importance are electron capture by protons (and protons bound in nuclei), neutrino production through electron-positron pair annihilation, and neutrino-electron scattering.

In recent years, with the experimental evidence pointing strongly to the existence of neutrino oscillations, it is also important to investigate the possible role of flavor-changing interactions to the supernova problem. Investigation into this has begun,²⁶ but has yet to be incorporated in a detailed simulation.

3. V2D: A New Code for Two-Dimensional Radiation Hydrodynamics

Our new radiation-hydrodynamic simulation code, V2D, is a two-dimensional, Newtonian, pure Eulerian, staggered-mesh code based on a modified version of the algorithm for ZEUS-2D by Stone and Norman.^{23,24,25} Following Stone and Norman, it has been designed for use in a general orthogonal two-dimensional geometry, which makes its utility extend beyond the supernova problem.

V2D is an entirely new implementation, coded according to the Fortran 95 standard. It is a distributed-memory parallel code that uses calls to MPI-1 for message passing between processes. It has been designed for easy portability between computing platforms and currently runs on systems ranging from as small as a Linux-based laptop to as many as 2048 processors of an IBM SP. To aid in this portability, the input and output is formatted using parallel HDF5, which is built on the MPI-I/O portion of the MPI-2 standard.

One of the major design goals of V2D is componentization and, to adhere to this principle, we insist on completely separating microphysics from the numerical implementation of our radiation-hydrodynamics algorithm. This isolation of mathematics and computational science from physics has allowed significant contributions from applied mathematicians to enhancing the performance of our code.

The V2D algorithm relies on operator splitting, with advection steps split from source-term steps. Hydrodynamic and neutrino-transport source-term steps and coupling are interleaved. At the start of each simulation timestep, the gravitational mass interior to each point is calculated. Since the collapsed core is nearly spherically symmetric and highly condensed, we approximate the gravitational mass assuming that mass interior to the point of interest is in a spherically symmetric distribution. In future versions of our code, we will implement a more accurate Poisson solver to calculate the (slightly) non-spherical gravitational potential.

In a break from Stone and Norman’s method, V2D next performs the advection sweeps in the radiation-hydrodynamic quantities (mass density, matter internal energy, velocities and momenta, electron fraction, and neutrino distributions). Following this, a neutrino transport step is performed for each flavor and each matter-radiation energy exchange is calculated.

The matter pressure is next updated, upon which the gravitational and matter- and radiation-pressure forces are applied to the matter. Artificial viscosity is calculated next and its contributions applied to the fluid. Finally, the gas-energy equation is solved.

This procedure is repeated for each timestep in a simulation, with the provision that advection sweeps are ordered alternately according to timestep (*i.e.*, x_1 -direction first, followed by x_2 , or *vice versa*).

3.1. Neutrino Transport Implementation

As an extension of earlier work by us,^{21,30} we implement neutrino transport by taking the zeroth angular moment of the BTE to yield the following neutrino monochromatic energy equation in the co-moving frame:

$$\frac{\partial E_\varepsilon}{\partial t} + \mathbf{V} \cdot (E_\varepsilon \mathbf{v}) + \mathbf{V} \cdot \mathbf{F}_\varepsilon - \varepsilon \frac{\partial}{\partial \varepsilon} (\mathbf{P}_\varepsilon : \mathbf{V} \mathbf{v}) = \mathbb{S}_\varepsilon, \quad (6)$$

where E_ε is the neutrino energy density per unit energy interval at position \mathbf{x} and time t , \mathbf{F}_ε is the neutrino energy flux per unit energy interval, and \mathbf{P}_ε and \mathbb{S}_ε are as defined earlier. The expression $\mathbf{P}_\varepsilon : \mathbf{V} \mathbf{v}$ indicates contraction in both indices of the second-rank tensors \mathbf{P}_ε and $\mathbf{V} \mathbf{v}$. There is a corresponding equation to describe the antineutrinos. This pair of equations is repeated for each neutrino energy ε , and neutrino flavor. We currently track electronic, muonic, and tauonic neutrinos.

Equation (6) is closed using Levermore and Pomraning’s prescription for flux-limited diffusion,¹⁶ which allows us to express \mathbf{F}_ε as

$$\mathbf{F}_\varepsilon = -D_\varepsilon \nabla E_\varepsilon, \quad (7)$$

where D_ε is a “variable” diffusion coefficient that varies in such a way as to yield the correct fluxes for the diffusion and free streaming limits and an approximate solution in the intermediate regime. This prescription also provides the elements of the radiation-pressure tensor \mathbf{P}_ε .

Presently, we employ the same prescriptions for electron capture and conservative scattering that we have used in the past.^{21,2} The rates for these process are calculated on the fly within the course of a simulation. Our model also implements neutrino production via electron-positron pair annihilation, as in Yueh and Buchler³⁴ and Bruenn². Neutrino-electron scattering has been implemented, but is not currently turned on in the preliminary results we present here. These latter two sets of processes use tables of precomputed rates, which are interpolated via a tri-linear interpolation scheme over neutrino energy ε , temperature T , and electron chemical potential μ_e .

Since the neutrino CFL restriction on a transport timestep is far too restrictive to permit an explicit solution, we use a purely implicit method to solve the transport. The equations comprising the description of each neutrino-antineutrino species are assembled in matrix form. We note

that the second (advective) term in Eq. (6) is omitted from this process since it has been already treated during the operator splitting of the advective step described above. Blocking terms arising from Fermi-Dirac statistical restrictions on final neutrino states make this a system of non-linear equations. Fortunately, the system is sparse, which makes it amenable to solution by sparse iterative methods. A nested procedure is used, employing Newton-Krylov methods³⁰. In the innermost loop, a linearized system is solved using preconditioned Krylov-subspace methods. The outer loop uses a Newton-Raphson iterative scheme to resolve the non-linearity of the system. Besides being an effective general procedure for sparse systems, our implementation of parallel preconditioners also insures that is amenable to large-scale solution on parallel architectures. This is the chief reason our code exhibits its high degree of scalability across many platforms.

3.2. Equation of State

V2D is designed to use an arbitrary equation of state and we use several in the course of testing the code. For production runs, however, we use the Lattimer-Swesty EOS^{15,14} in tabular form. The thermodynamic quantities are tabulated in terms of independent variables, density, ρ , temperature, T , and electron fraction, Y_e . We have tabulated this EOS in a thermodynamically consistent way according to the prescription in Swesty²⁸. (We refer to this combination collectively as LS-TCT.) We note that although the Lattimer-Swesty EOS is commonly used, and tabulations of it are also common, most tabulations are not constructed in such a way as to *guarantee* thermodynamic consistency. When non-thermodynamically-consistent tables are used, spurious entropy can be generated or lost. Such problems have been sometimes incorrectly attributed to the Lattimer-Swesty EOS, rather than erroneous tabulation of the otherwise consistent EOS.

To guarantee tabular thermodynamic consistency, LS-TCT uses bi-quintic Hermite interpolation in the Helmholtz free energy F , as a function of T and ρ . Functional dependence on Y_e changes slowly enough to permit linear interpolation. This procedure is required since satisfaction of the Maxwell relations requires consistency among the second derivatives of F . In addition, we desire fidelity of the interpolation and continuity of derivatives to the underlying tabular data for both F and its derivatives, $(\partial F/\partial T)_\rho$ and $(\partial F/\partial \rho)_T$.

Apart from thermodynamic considerations, we also want to insure that there are no discontinuities that might cause difficulties in the hydrodynamics. Hence, LS-TCT also insists that interpolations of the second derivatives of F approach the correct tabulated values. (This is the equivalent of saying that we require the derivatives of pressure and internal energy with respect to temperature and density be continuous.)

A final requirement is that we wish the interpolation function and its first and second derivatives be continuous across table-cell boundaries. This insures that nothing untoward happens as a fluid element migrates from one thermodynamic regime of interest to another.

3.3. Software Validation and Verification

When engaged in a major project, such as V2D, it is important for software developers to be constantly vigilant about the quality of software being produced. It is important that the software meet the requirements that it is intended to address (validation) and that the code yields correct answers (verification).

We take these issues seriously and, in an effort to address them, have implemented strict source-code control and testing procedures to ensure that our software meets our rigorous standards. One of the most important elements of our program has been the implementation of a suite of regression tests, which we currently run four times daily. This is not a static suite, but is constantly growing.

Our eventual aim is to cover every major element of code in V2D. Currently our suite consists of about two dozen separate problems that include tests of the hydrodynamics, neutrino transport, parallel solvers, message passing, and parallel I/O. Wherever possible, we try to include problems with analytic or at least verifiable solutions.

Although implementation of these procedures is labor intensive and time-consuming, we feel it is a justifiable investment. With current regression tests, our procedures have already been effective in finding errors in our code. They have also served as an effective safeguard against introducing new errors as we continually enhance V2D’s functionality.

4. Initial Results

We are using V2D to carry out our first 2-D multigroup models of the post-bounce epoch. To date, simulations have not reached a sufficient time that would allow us to be certain about whether an explosion is obtained. Nevertheless, the results warrant some discussion as they reveal important features of the post-bounce epoch.

4.1. Initial Model

For a progenitor model we employ the widely-used Woosley and Weaver³³ S15S7B2 $15M_{\odot}$ progenitor. Much previous work has focused on the evolution of this progenitor through collapse, core bounce, and convective phases. The Fe core, the Si shell, and a portion of the O shell area are zoned into a 256 radial-mass-zone mesh with zoning that is tuned (by trial and error) so as to yield a high spatial resolution grid in the proto-neutron star and the inner 200 km of the collapsed core at bounce. This tuned zoning sets up a radial grid that is compatible with subsequent 2-D Eulerian simulations. The neutrino-energy spectrum, ranging from 0–375 MeV, is discretized into 20 energy groups with group widths that increase geometrically with energy so as to resolve accurately the Fermi surface of the electrons and neutrinos in the proto-neutron star. The initial values for T , ρ , and Y_e , are interpolated from the original S15S7B2 data onto the Lagrangean mass grid and the initial radial coordinates of each mass shell are computed consistently with density. The neutrino energy densities E_{ν} are initialized to a small non-zero value that yield an initial neutrino luminosity that is many orders of magnitude below what the precollapse thermal pair-production luminosity would be. When the simulation is started in its pre-collapse quasi-static phase, the luminosity stabilizes within a light crossing time (5-10 ms).

4.2. Lagrangean Collapse Calculations

The initial model is collapsed using a 1-D Newtonian Lagrangean radiation hydrodynamics code RH1D that uses the mass and energy meshes described above. The evolution algorithm for each timestep utilizes operator splitting to first carry out a Lagrangean hydrodynamics step followed by Lagrangean neutrino evolution steps for each of the three neutrino flavors. After each Lagrangean neutrino evolution step the matter internal energy and electron fraction are corrected for any energy and lepton number exchange that has occurred.

The model contains neutrino microphysics as described in Bruenn² with two exceptions. The neutrino-nuclei scattering opacity has been modified to take into account the form-factor introduced by Burrows, Mazurek, and Lattimer⁶ and we have neglected the effect of neutrino/anti-neutrino annihilation. Full neutrino-electron scattering as described in this paper is included in the code but is not turned on in the model described in this paper. Additional effects such as nucleon recoil, ion-ion correlations, etc. are being considered as follow-ons to this baseline model.

The EOS utilized is the TCT tabularized version of the nuclear EOS Lattimer-Swesty (LS-TCT) with the $k = 180$ MeV parameter set, with the exception of the electron EOS that has been updated to improve accuracy and the range of applicability. The original LS EOS chose a value for the alpha particle binding energy $B_\alpha = 28.3$ MeV that did not correctly account for the neutron-proton mass difference. This parameter has been subsequently corrected but in the model presented in this paper, the original value has been retained so as to allow comparison to other work.

Using RH1D with the microphysics and meshes described above the core collapses in approximately 233 ms. The central conditions at bounce are approximately $T \approx 10.3$ MeV, $\rho \approx 2.71 \times 10^{14}$ g cm $^{-3}$, $Y_e \approx 0.306$, and $Y_\ell \approx 0.37$. These conditions are in good agreement with those obtained in Lagrangean MGFLD and MGBT models^{2,21,27,19}.

4.3. Eulerian 2-D Calculations

Our 2-D models are carried out in spherical polar coordinates. The initial conditions for our 2-D simulations are taken from the 1-D Lagrangean simulations as the central density of the core reaches the nuclear saturation density. The T , ρ , and Y_e profiles at this point are shown in Figure 1 and are taken at approximate time of 233.087 ms. The choice of this epoch to begin our 2-

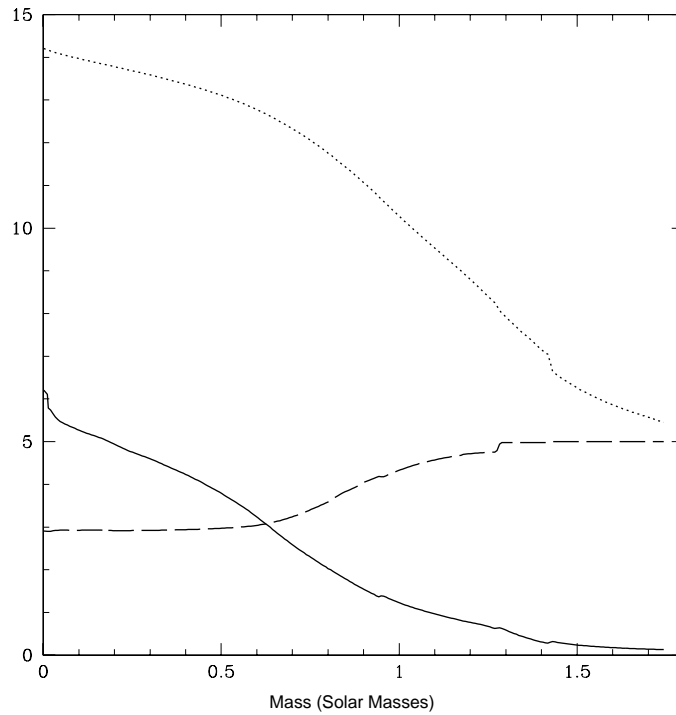


Figure 1. Initial radial profile for 2-D simulation. Solid line indicates temperature in units of MeV. Dashed line indicates $10 \times Y_e$. Dotted line indicates $\log_{10}(\rho)$ in units of g cm $^{-3}$.

D models was made for two reasons. First, the prompt shock propagates and stalls into a quasi-static equilibrium on the Eulerian mesh. We have found that if we attempt the transition from a Lagrangean algorithm to an Eulerian algorithm at the point where the shock has stalled, there will be noticeable differences in the quasi-static equilibrium caused by the presence of the nuclear “pasta” phase transition. These differences in the equilibrium point can set off spurious unphysical

shocks. By choosing to let the prompt shock propagate a stall on an Eulerian mesh, we avoid this problem. The second reason for choosing the initial point for our 2-D models near the moment of bounce is that the radial coordinates of the zones in the outer part have achieved desirable values for an Eulerian simulation.

The radial zoning for the 2-D models is taken directly from the radial coordinates of the 1-D Lagrangean model zones. In this way we avoid any need for remapping of data between radial zones. This eliminates the introduction of any spurious forces into the initial conditions for the 2-D models. The initial data for T , ρ , Y_e , v_r , and the neutrino energy densities E_ν and \bar{E}_ν for each neutrino flavor are taken directly from the 1-D Lagrangean model. The initial velocity in the θ direction is set to zero. The data are mapped in the polar-angular direction in a spherically symmetric fashion. The angular grid consists of 256 zones uniformly spaced in angle over the range of $0 \leq \theta \leq \pi$. We place a small sinusoidal perturbation in the electron fraction Y_e to seed convection in the region between 100 and 200 km of the form $(Y_e)_{\text{perturb}} = (Y_e)_{\text{Lagrangean}} + C_p \sin(4\theta)$ where $C_p = 10^{-6}$. The energy group structure is also left unchanged from the 1-D Lagrangean runs so there is no need to remap the data in the energy dimension. In the remainder of this paper we shall refer to this model as Production Run 37 (PR37).

The use of spherical polar coordinates in combination with explicit hydrodynamic algorithms to model spatial domains that include the origin gives rise to a numerical stability problem. At $r = 0$ the spherical coordinate system is degenerate and all zones that include the origin as a vertex should be in instantaneous sonic communication with one another. However, standard explicit numerical finite-difference, finite-volume, or finite-element techniques are limited to nearest-neighbor type spatial coupling and do not include numerical coupling between all zones containing a given vertex. In order to circumvent this problem we numerically introduce “baffles” into the center of the collapsed core, as though it were a tank of fluid, to prevent movement of fluid in the angular direction inside a certain radius. Since no fluid movement occurs in the θ direction inside the baffle radius, there is no CFL restriction based on the zone size in the θ direction for zones inside that radius. Nevertheless, the zones on either side of the baffle are sonically connected as sound waves flow around the outer edge of each baffle. We strive to keep the baffle radius small, so that the flow in the θ direction remains unimpeded in any region where convective instabilities may develop. For the mode described in this paper the baffle radius is approximately 8.5 km which yields an average CFL timestep of about 5×10^{-7} s. As we will see, this baffle radius is well inside of any proto-neutron star (PNS) instability region.

The 2-D calculations have been carried out on the IBM-SP system at the National Energy Research Scientific Computing Center (NERSC). The models are run on 1024 processors with parallelism handled via message passing via calls to MPI libraries. Model PR37 required approximately 50,000 processor-hours of CPU time to reach a simulation time of 16 ms post-bounce.

4.4. *The Onset of Convection*

The 2-D models are carried out from the point of bounce. As expected the prompt shock weakens while propagating outward and finally stalls. In the 2-D models, the radius of the shock at 5 ms post-bounce is near 60 km and propagating outwards very slowly. This is in good agreement with our 1-D Lagrangean models.

One difference that we see from previous works including the grey models carried out by Swesty²⁹ is that convective instabilities are born much earlier when the 2-D models are initialized near the point of core bounce. By 10 ms after bounce, the model has developed two separate unstable layers. The outer layer, shown in Fig. (2), is the classic entropy driven Rayleigh-Taylor

convection.

The inner layer, shown in Fig. (3), seems to be an instability in the outer layers of the proto-neutron star similar to those seen in 2-D simulations carried out by Keil *et al.*¹³ and Mezzacappa *et al.*²⁰.

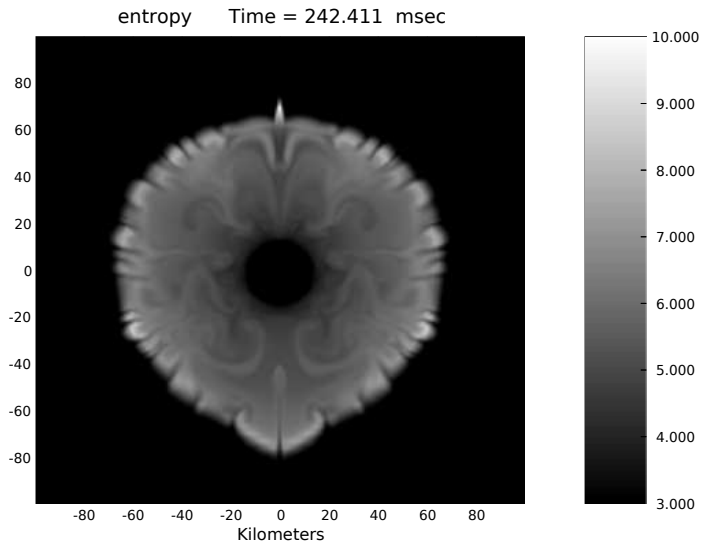


Figure 2. The entropy per baryon for model PR37 at approximately 9 ms after core bounce.

There is controversy about the existence of PNS instabilities. Originally, the work by Wilson and Mayle^{32,31} claimed to find doubly-diffusive instabilities in the region below the neutrinosphere. Later work by Bruenn and collaborators^{3,4,5} cast doubt on the existence of such phenomena. The simulations of Keil,¹³ which utilized the grey flux-limited diffusion approximation to transport neutrinos along radial rays, found a PNS instability that grew over the time period of approximately one second to encompass the entire proto-neutron star. In contrast, the subsequent work of Mezzacappa *et al.*²⁰ found a PNS instability that quickly damped out within a short time. The Mezzacappa *et al.* simulation utilized a multigroup flux-limited P_1 approximation to transport neutrinos along radial rays outward from an inner radius of $r=20$ km. The inner boundary conditions in this simulation were established as time-dependent data from the 1-D Lagrangean code of Bruenn². It is important to note that neither the simulations of Keil *et al.*¹³ or Mezzacappa *et al.*²⁰ took into account the fully radiation-hydrodynamic coupling via the compression and dynamic diffusion terms that are present in Eq. (6). Our simulations have confirmed the expected result that the effects of the dynamic diffusion term dominate the radiative diffusion term in the regions in which the optical depth is large.

Figure 3 shows the instantaneous structure of the velocity field in model PR37 at the same time as the data shown in Fig. (2). The velocity field is illustrated by means of a Lagrangean-Eulerian Advection (LEA) visualization technique that shows the direction of the vectors as streaks. One can clearly see eddies associated with the PNS instability layer at a radius of about 20–25 km. This is well outside the baffle radius of 8.5 km. In fact, there are approximately a minimum of 40 radial zones separating the innermost of the vortices and the outer edge of the baffles. We do not believe

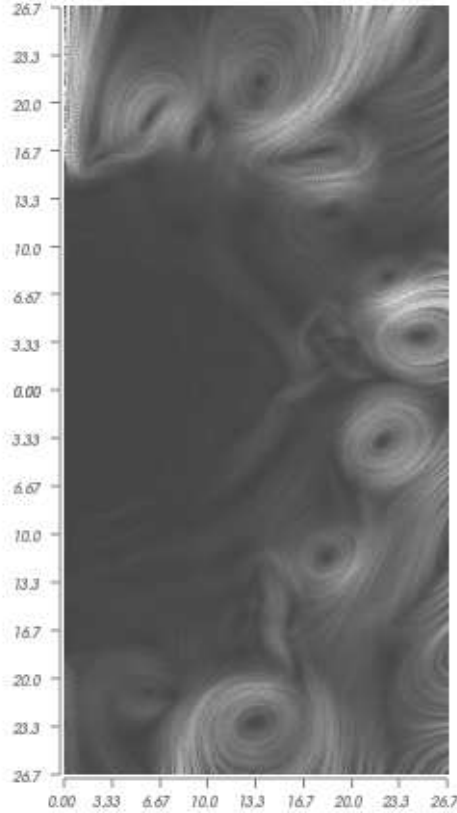


Figure 3. The velocity structure of the PNS instability layer in model PR37 at $t=242.411$ ms. The image depicts the instantaneous structure of the velocity field by means of a texture map visualization technique known as Lagrangean-Eulerian Advection (LEA).

that the baffles in any way impede the dynamics of the vortices. Nevertheless other simulations are underway where the baffle radius is made substantially smaller to verify this claim. We are also developing an implicit hydrodynamic algorithm that will avoid the need for baffles altogether.

Whether the PNS instability will grow or diminish with time is as yet unclear since we have only evolved model PR37 to a time of approximately 16 ms at the time of this writing. The velocity structure at that time is shown in Fig. (4), which clearly reveals that much coherency has been lost in the vortical structure of the PNS instability layer. This seems indicative of the decay of this PNS instability in a fashion similar to that described by Mezzacappa *et al.*²⁰. However, it is necessary to evolve this simulation substantially farther in time before any definitive statements can be made about the long-term behavior of this sector of the proto-neutron star. During this relatively short timescale the outer convective zone seen in Fig. (2) does not exhibit significant growth. With evolution to the next 30 ms, we should be able to make comparative statements regarding model PR37 and earlier grey models carried out by Swesty²⁹.

5. Conclusions and Future Directions

The issues and work described in this paper fall far short of offering complete coverage of the active issues that remain in the area of the explosion mechanism of core collapse supernovae. Indeed, we

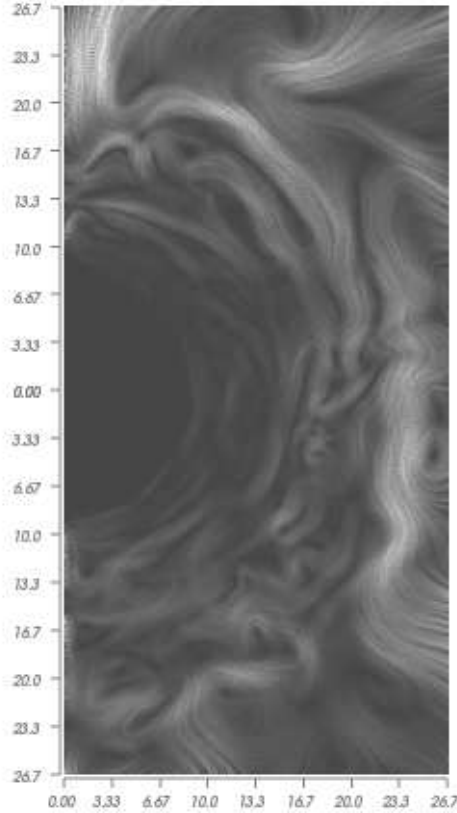


Figure 4. The velocity structure of the PNS instability layer in model PR37 at $t=249.177$ ms.

have ignored many important issues such as magnetic fields, rotation, and neutrino flavor mixing. Clearly there is a large gulf of unexplored physics incorporated in those subjects.

Our own future efforts will be focused in two areas in the near future. The first of these is understanding the effects of numerous microphysics enhancements that will be added to the models. The second of these efforts involves extending the models to 3-D where a more realistic convective flow structure can arise.

Acknowledgments

The authors would like to thank Ed Bachta and Polly Baker of Indiana University at Indianapolis for their collaborative efforts in developing the visualization technology that went into Figures 3 and 4. We gratefully acknowledge the support of the U.S. Dept. of Energy, through SciDAC Award DE-FC02-01ER41185, by which this work was funded. We are also grateful to the National Energy Research Scientific Computing Center (NERSC) for computational support. Finally, we would like to thank the National Institute for Nuclear Theory at the University of Washington for its hospitality in hosting the workshop “Open Issues in Core-Collapse Supernovae,” at which this work was presented in June 2004.

References

1. R. L. Bowers and J. R. Wilson, *Astrophys. J. Supp.*, **50**, 115 (1982).
2. S. W. Bruenn, *Astrophys. J. Supp.*, **58**, 771 (1985).
3. S. W. Bruenn and A. Mezzacappa, *Astrophys. J.*, **433**, L45 (1995).
4. S. W. Bruenn, A. Mezzacappa and T. Dineva, *Phys. Rep.*, **69**, 256 (1995).
5. S. W. Bruenn and T. Dineva, *Phys. Rep.*, **458**, L71 (1996).
6. A. Burrows, Mazurek, T. J. and J. M. Lattimer, *Astrophys. J.*, **251**, 325 (1981).
7. J. Cooperstein, L. J. van den Horn and E. Baron, *Astrophys. J.*, **309**, 653 (1986).
8. D. Z. Freedman, *Phys. Rev. D.*, **9**, 1389 (1974).
9. C. L. Fryer and M. S. Warren, *Astrophys. J.*, **601**, 391 (2004).
10. M. Herant, W. Benz, R. Hix, C. L. Fryer and S. A. Colgate, *Astrophys. J.*, **435**, 339 (1994).
11. R. Hix, personal communication, 2004.
12. H.-T. Janka, R. Buras, K. Kifonidis, T. Plewa and M. Rampp, in *From Twilight to Highlight: The Physics of Supernovae*, eds. W. Hillebrandt and B. Leibundgut, Springer, Berlin, 2003.
13. W. Keil, H.-T. Janka, and E. Muller, *Astrophys. J.*, **473**, L111 (1996).
14. Lattimer, J. M., C. J. Pethick, D. G. Ravenhall, and D. Q. Lamb, *Nucl. Phys. A*, **432**, 646 (1985).
15. Lattimer, J. M. and F. D. Swesty, *Nucl. Phys. A*, **535**, 331 (1991).
16. C. D. Levermore and G. C. Pomraning, *Astrophys. J.*, **248**, 321 (1981).
17. E. Livne, A. Burrows, R. Walder, I. Lichtenstadt and T. Thompson, *Astrophys. J.*, **609**, 277 (2004).
18. A. Mezzacappa and S. W. Bruenn, *Astrophys. J.*, **405**, 669 (1993).
19. A. Mezzacappa and S. W. Bruenn, *Astrophys. J.*, **405**, 685 (1993).
20. A. Mezzacappa, A. C. Calder, S. W. Bruenn, J. M. Blondin, M. W. Guidry, M. R. Strayer and A. S. Umar, *Astrophys. J.*, **493**, 848 (1998).
21. E. S. Myra, S. A. Bludman, Y. Hoffman, I. Lichtenstadt, N. Sack and K. A. Van Riper, *Astrophys. J.*, **318**, 744 (1987).
22. M. Ramp and H.-T. Janka, *Astron. & Astrophys.*, **396**, 361 (2002).
23. J. M. Stone and M. L. Norman, *Astrophys. J. Supp.*, **80**, 753 (1992).
24. J. M. Stone and M. L. Norman, *Astrophys. J. Supp.*, **80**, 791 (1992).
25. J. M. Stone, D. Mihalas and M. L. Norman, *Astrophys. J. Supp.*, **80**, 819 (1992).
26. P. Strack and A. Burrows, *Phys. Rev. D.*, **71**, 093004 (2005).
27. F. D. Swesty, J. M. Lattimer and E. S. Myra, *Astrophys. J.*, **425**, 195 (1994).
28. F. D. Swesty, *J. Comp. Phys.*, **127**, 118 (1996).
29. F. D. Swesty, in *Stellar Evolution, Stellar Explosions and Galactic Chemical Evolution*, ed. A. Mezzacappa, Institute of Physics Publishing, Bristol, p. 539, (1998).
30. F. D. Swesty, D. C. Smolarski and P. E. Saylor, *Astrophys. J. Supp.*, **153**, 369 (2004).
31. J. R. Wilson and R. W. Mayle, *Phys. Rep.*, **227**, 97 (1983).
32. J. R. Wilson and R. W. Mayle, *Phys. Rep.*, **163**, 63 (1988).
33. S. E. Woosley and T. A. Weaver, *Astrophys. J. Supp.*, **101**, 181 (1995).
34. W. R. Yueh and J. R. Buchler, *Astrophys. & Space Sci.*, **39**, 429 (1976).